Band structure and optical properties of Si-$Si_{1-x}Ge_x$ superlattices

Y. Rajakarunanayake and T. C. McGill
California Institute of Technology, Pasadena, California 91125
(Received 9 February 1989)

We report the band structure and optical properties of Si-$Si_{1-x}Ge_x$ superlattices calculated by $\mathbf{k}\cdot\mathbf{p}$ theory using the envelope-function approximation. In this paper we have demonstrated that direct-band-gap Si-$Si_{1-x}Ge_x$ superlattices can be achieved by a suitable choice of layer thicknesses. We have presented detailed results for Si-$Si_{0.5}Ge_{0.5}$ superlattices grown on $Si_{0.75}Ge_{0.25}$ buffer layers with layer thicknesses in the range from 4 to 24 monolayers. Our calculations indicate that the optical absorption strengths can vary by 3–4 orders of magnitude even for layer thickness variations as small as 1–2 monolayers. Thus, it is important to control the layer thicknesses to a monolayer accuracy to obtain the enhanced optical absorption strengths. Although these optical absorption strengths are 3–4 orders of magnitude larger than bulk Si or Ge, they are still 3 orders of magnitude smaller than the absorption strengths due to direct transitions in materials such as GaAs.

I. INTRODUCTION

Silicon and germanium have been extremely important materials in the field of semiconductor electronics for the past few decades. Traditionally Si has been the material of choice for semiconductor electronics not only because of its electronic properties, but also because of its superior mechanical properties and the excellent insulating qualities of its oxide.[1] However, due to their indirect band gaps, Si and Ge have not been suitable for optoelectronic applications. The optical absorption strengths of pure Si and Ge are about 6 orders of magnitude lower than a typical optoelectronic material such as GaAs.[2] However, recent advances in crystal-growth techniques such as molecular-beam epitaxy (MBE) have allowed the fabrication of layered epitaxial structures known as superlattices.[3] In particular the Si-$Si_{1-x}Ge_x$ superlattices seem to offer the intriguing possibility of greatly enhancing the optical properties over pure Si or Ge.[4–14] A typical Si-$Si_{1-x}Ge_x$ superlattice grown in the [001] direction can be considered as a crystal with an extended unit cell along the growth axis. This has the consequence of reducing the Brillouin zone in the growth direction and qualitatively folding the bulk energy band into the reduced zone. For materials such as Si and Ge, this raises the possibility of tailoring the folding of the indirect conduction band. If the folded Δ minimum can be brought to the zone center Γ, the resulting band structure would be direct.[9] In such a case there will be (Γ_V-Γ_C) direct optical transitions allowed between the top of the valence band and the bottom of the direct conduction band. We have estimated that superlattice ordering induced direct optical transition rates in Si-$Si_{1-x}Ge_x$ superlattices can be 3–4 orders of magnitude stronger than in phonon-assisted optical absorption of pure Si and Ge. A major issue of interest then is whether such quasidirect Si-$Si_{1-x}Ge_x$ superlattices are promising candidates for optoelectronic devices. We also discuss a simple criterion for obtaining approximately direct band structure given by

$$k_{\min}^{\mathrm{Si}} d^{\mathrm{Si}} + k_{\min}^{\mathrm{Si}_{1-x}\mathrm{Ge}_x} d^{\mathrm{Si}_{1-x}\mathrm{Ge}_x} \approx 2n\pi + \delta \ . \quad (1)$$

Here, d^{Si} and $d^{\mathrm{Si}_{1-x}\mathrm{Ge}_x}$ are the layer thicknesses of the constituent layers, $k_{\min}^{\mathrm{Si}}$ and $k_{\min}^{\mathrm{Si}_{1-x}\mathrm{Ge}_x}$ are wave vectors of the longitudinal Δ_1^{lc}-valley minima, and δ is a phase shift that is independent of the layer thicknesses.

In Sec. II of this paper we have briefly outlined the full-zone $\mathbf{k}\cdot\mathbf{p}$ theory[15] used to calculate the band structure and optical properties of Si-$Si_{1-x}Ge_x$ superlattices. We have performed the calculations of the superlattice band structure in the envelope-function approximation (EFA). Although the EFA has been used for the study of the conduction bands of Si-$Si_{1-x}Ge_x$ by earlier investigators,[16] this work is the first study on the optical properties of the Si-$Si_{1-x}Ge_x$ system based on the EFA. Section III is devoted to a brief discussion of the role of strain in determining the alignments of the various bands in coherently strained Si-$Si_{1-x}Ge_x$ superlattices. We outline a novel method of describing the motion of the conduction bands with strain, by incorporating appropriate deformation potentials at the zone center. In Sec. IV we analyze the superlattice band structure for a few illustrative cases, and discuss the main features of the band structure of indirect superlattices. A new result we find in Si-$Si_{1-x}Ge_x$ superlattices is that the lowest conduction band splits into a doublet due to an interference effect between the electrons from the two longitudinal valleys. In Sec. V we describe the calculations of the optical properties based on the envelope-function approximation. Our calculations indicate that the optical absorption strengths can change over 3–4 orders of magnitude for layer thickness variations as small as 1–2 monolayers. In Sec. VI, we summarize the general conclusions for Si-$Si_{1-x}Ge_x$ superlattices.

II. THEORY

In this paper we have investigated the possibility of engineering a direct-band-gap superlattice within the framework of a full-zone $\mathbf{k}\cdot\mathbf{p}$ theory. The $\mathbf{k}\cdot\mathbf{p}$ method is par-

ticularly suitable for the calculation of the optical properties because of its ability to directly calculate various optical matrix elements. We have used the full-zone $\mathbf{k}\cdot\mathbf{p}$ theory introduced by Cardona and Pollack[15] to calculate the bulk band structure of Si and Ge. The parameters for the calculation of unstrained band structures of Si and Ge are taken from Cardona and Pollack.[15] To accurately represent the strained band structures of Si and Ge we have slightly modified the zone-center energies. The properties of $Si_{1-x}Ge_x$ alloys were determined by a linear interpolation of the $\mathbf{p}$-matrix elements and the zone-center energies of Si and Ge.

It is well known that the wave function at an arbitrary point in the Brillouin zone can be expanded in terms of a linear combination of the zone-center basis set. We have kept the lowest 15 zone-center basis states corresponding to the [000], eight $[\frac{1}{2}\frac{1}{2}\frac{1}{2}]$, and six [001] plane waves of an empty fcc reciprocal lattice. In the notation of group theory, the irreducible representations of these 15 states correspond to the three threefold-degenerate representations $\Gamma_{15},\Gamma^u_{25'},\Gamma^l_{25'}$, one twofold representation Γ_{12}, and four onefold representations $\Gamma^u_1,\Gamma^l_1,\Gamma^l_{2'},\Gamma^u_{2'}$. In Table I we have given the values used for the zone-center energies in our calculations. We have used atomic units throughout this work to express our results. The momentum operator $\mathbf{p}=-i\nabla$ is a vector operator and thus belongs to the Γ_{15} irreducible representation of the O_h^7 $(Fd3m)$ space group. The application of group theory dictates that there are only ten independent momentum matrix elements between the 15 zone-center basis states. In Table II, we have enumerated the values of these momentum matrix elements appropriate for bulk Si and Ge.

In the [001] direction, the 15×15 $\mathbf{k}\cdot\mathbf{p}$ Hamiltonian can be block diagonalized into one 5×5, three 3×3, and one 1×1 submatrice. The bottom of the conduction band in the [001] direction ($\Delta_1^{\rm lc}$) is then given by the second largest eigenvalue of the following 3×3 matrix:

$$\begin{bmatrix} E_{15}+k_z^2 & k_zT & k_zT' \\ k_zT & E_1^u+k_z^2 & 0 \\ k_zT' & 0 & E_1^l+k_z^2 \end{bmatrix}. \tag{2}$$

The top of the valence band in the [001] direction (Δ_5^v) is given by the second largest eigenvalue of the following 3×3 matrix:

$$\begin{bmatrix} E^l_{25'}+k_z^2 & k_zQ & 0 \\ k_zQ & E_{15}+k_z^2 & k_zQ' \\ 0 & k_zQ' & E^u_{25'}+k_z^2 \end{bmatrix} \tag{3}$$

The matrices of Eqs. (2) and (3) are expressed in atomic units in which the unit of length is the Bohr radius, $\hbar$ is the unit of action, and the rydberg is the unit of energy. In these fundamental units, the unit of mass becomes $\frac{1}{2}$ times the electron rest mass and the charge of an electron $\sqrt{2}$. The parameters used for the actual calculations are presented in Tables I and II.

The light-particle band at the top of the valence band $\Delta_{2'}^v$ is given by a root of the 5×5 submatrix.[15] The presence of the spin-orbit interaction complicates the situation by doubling the size of the Hamiltonian matrix from 15×15 to 30×30. However, the main effect of the k-independent part of the spin-orbit interaction is to couple one Δ_5^v heavy particle and the $\Delta_{2'}^v$ light particle from the threefold degenerate $\Gamma^l_{25'}$ valence-band edge to give the conventional light hole and the spin-orbit split-off bands. However, the other Δ_5^v heavy-particle band remains the same in the presence of the spin-orbit interaction to give the conventional heavy-hole band. The identification of the heavy-hole band to the Δ_5^v band can be made even in the presence of diagonal strain. For most of this work we have focused our attention on only the heavy-band and the longitudinal $\Delta_1^{\rm lc}$ ellipsoids of the lowermost conduction bands since they are the relevant bands for near-band-gap optical transitions. For the purpose of our discussions we have denoted the longitudinal conduction band $\Delta_1^{\rm lc}$ by $|c\rangle$ and the heavy-hole bands Δ_5^v as $|v\rangle$. In the zone-center representation, both these states are column vectors of 15 elements with only three nonzero components. It is fairly easy to work out the optical matrix elements in this basis set, because the matrix elements of the 15×15 momentum operator are known. Our calculations indicate that for [001] grown superlattices, $\langle c|p_z|v\rangle=0$. However, $\langle c|p_x|v\rangle=\langle c|p_y|v\rangle\neq0$. Thus, only light polarized in a plane perpendicular to the

TABLE I. Matrix elements of the momentum operator $\mathbf{p}$ (in atomic units) used in the $\mathbf{k}\cdot\mathbf{p}$ calculations. The alloy properties are calculated by averaging the Si and Ge values.

$\mathbf{p}$-matrix element	Si	Ge
$P(2i\langle\Gamma^l_{25'}\|\mathbf{p}\|\Gamma^l_{2'}\rangle)$	1.20	1.36
$Q(2i\langle\Gamma^l_{25'}\|\mathbf{p}\|\Gamma_{15}\rangle)$	1.05	1.07
$R(2i\langle\Gamma^l_{25'}\|\mathbf{p}\|\Gamma_{12'}\rangle)$	0.830	0.8049
$P''(2i\langle\Gamma^l_{25'}\|\mathbf{p}\|\Gamma^u_{2'}\rangle)$	0.100	0.100
$P'(2i\langle\Gamma^u_{25'}\|\mathbf{p}\|\Gamma^l_{2'}\rangle)$	−0.090	0.1715
$Q'(2i\langle\Gamma^u_{25'}\|\mathbf{p}\|\Gamma_{15}\rangle)$	−0.807	−0.752
$R'(2i\langle\Gamma^u_{25'}\|\mathbf{p}\|\Gamma_{12'}\rangle)$	1.210	1.4357
$P'''(2i\langle\Gamma^u_{25'}\|\mathbf{p}\|\Gamma^u_{2'}\rangle)$	1.32	1.6231
$T(2i\langle\Gamma^u_1\|\mathbf{p}\|\Gamma_{15}\rangle)$	1.08	1.2003
$T'(2i\langle\Gamma^l_1\|\mathbf{p}\|\Gamma_{15}\rangle)$	0.206	0.5323

TABLE II. Zone-center regions (in rydbergs) used in the $\mathbf{k}\cdot\mathbf{p}$ calculations. The alloy properties are calculated by averaging Si and Ge values.

Zone-center state	Si	Ge
Γ_{25}^{l}	0.0000	0.0000
$\Gamma_{2'}^{l}$	0.2650	0.0728
Γ_{15}	0.2520	0.2320
Γ_{1}^{u}	0.5200	0.5710
Γ_{1}^{l}	−0.9500	−0.9660
$\Gamma_{12'}$	0.7100	0.7700
$\Gamma_{25'}^{u}$	0.9400	1.2500
$\Gamma_{2'}^{u}$	0.9900	1.3500

superlattice growth axis is allowed to induce optical transitions.

To study the band structure of Si-$Si_{1-x}Ge_x$ superlattices it is necessary to work out the complex band structure of the constituent bulks. The bulk Hamiltonian can be viewed as a quadratic function of a scalar parameter k_z (for the case $k_x=k_y=0$) involving 15×15 matrices. It can be shown that one can recast the problem of finding k_z to an eigenvalue problem double the size of the original Hamiltonian when E, k_x, and k_y are specified.[17,18] We have used this method in the calculation of the complex band structures of the constituent bulks.

The superlattice band structure is calculated in the multicomponent envelope-function approximation. The eigenstates we find from $\mathbf{k}\cdot\mathbf{p}$ theory can be propagated from one interface to the other within a given bulk layer. However, to match the wave functions across the interface, we need to impose boundary conditions on the wave functions and their normal derivatives. The first matching condition we used was that, for each wave function, the zone-center components are the same across the interface. This assumption can be justified by the observation that a perfect interface cannot change the symmetry of a zone-center wave function; each symmetry component has an equal magnitude on both sides of the interface.[17] The second condition is to match the current carried by each wave function to be the same on both sides of the interface. This is an important condition that has to be satisfied to preserve charge conservation at the interfaces. Finally, we impose the Bloch condition that relates the amplitude of the wave function at a given point in a superlattice unit cell to the amplitude in an adjacent cell at the same corresponding point by a factor of the form $e^{iQ(d_1+d_2)}$. Here d_1 and d_2 are layer thicknesses within a single period of the superlattice, and Q denotes the superlattice wave vector within the reduced Brillouin zone. The Bloch condition can be cast into an eigenvalue problem whose solution gives the values of the superlattice wave vector Q.

It is important to note that, in typical calculations of the complex band structure by the $\mathbf{k}\cdot\mathbf{p}$ method, the physical solutions are usually accompanied by several unphysical solutions that have to be discarded.[17,19] We identify these unphysical solutions if the energy bands are purely imaginary or complex in the energy range of interest (-5 eV to $+5$ eV centered around the top of the valence-band edge). There are other bands that have to be discarded because their real parts do not lie within the first Brillouin zone. These spurious bands result from the inability of the $\mathbf{k}\cdot\mathbf{p}$ Hamiltonian to correctly mimic the periodic band structure in the repeated-zone scheme with the roots of a finite-order polynomial in k_z. Smith and Mailhiot[17] have shown that the correction terms from these neglected bands are quite small and on the order of 10^{-6} of the leading-order terms. We have consistently neglected the contributions to the band structure from these bands. Comparisons of calculations done with the tight-binding method and the envelope-function method based on GaAs systems have shown that the latter is fairly accurate even for ultrathin superlattices.[20] This justifies our application of the envelope-function approximation for the study of Si-$Si_{1-x}Ge_x$ superlattices.

III. BAND OFFSET AND STRAIN

Although Si and Ge surfaces are chemically compatible, there is $\approx4\%$ lattice mismatch between the two materials. This situation makes strain play an important role in determining the relevant band alignments between these two materials. The heterojunction band offset for Si/Ge interfaces has been investigated by several groups. Kuech *et al.*[21] estimated the band discontinuities from reverse-bias capacitance measurements to be $\Delta E_V=0.39\pm0.04$ eV. Margaritondo *et al.*[22] report a valence-band offset of 0.2 eV based on photoemission studies. Mahowald *et al.*[23] obtain 0.4 ± 0.1 eV based on the same technique. The theoretical predictions of Harrison[24] places the valence-band offset for Si/Ge at 0.38 eV. Tersoff[25] theory predicts a value of 0.18 eV. More recent predictions of Harrison and Tersoff[26] set the valence-band offset at 0.29 eV. The above predictions can be in substantial error because there has been no provision for the effects of strain.

However, recent *ab initio* density functional calculations by Van der Walle and Martin[27,28] have considered the effects of strain on the valence-band offsets explicitly. They find that the average positions of the valence-band edges of Si and Ge have an offset independent of strain $\Delta E_V^{\rm av}\approx0.54\pm0.04$ eV. People and Bean[29,30] have been able to obtain remarkable agreement with several experimental results for the band-edge positions of Si/Ge structures based on the valence-band offsets predicted by Van de Walle and Martin[27,28] combined with a phenomenological deformation potential theory. In this paper we have used a method similar to People and Bean[29,30] to obtain the heterojunction band alignments. Although there is still controversy about the value of the valence-band offset between Si and Ge, we expect the main features of the results discussed in this paper to be fairly independent of the value of the valence-band offset because of the extremely high effective masses of the longitudinal conduction bands.

The effects of strain on a threefold-degenerate Γ state can be easily included by the deformation potentials a, b, and d as introduced by Bir and Pikus.[31] In our calculations we have described the uniaxial splitting of the valence-band edge by the method described by

Hesagawa.[32] The effects of strain on the indirect conduction minima can be described by a uniaxial splitting and a hydrostatic shift with respect to the unstrained position of the valence-band edge.[32,33] According to the recent calculations of Van de Walle and Martin,[27,28] the hydrostatic deformation component of the valence-band offset is quite small. In other words, the offset between the average position of the valence bands of Si and Ge is roughly independent of strain. We have taken the deformation potential parameters for Si and Ge from Balslev.[34]

We have also done alternative calculations to characterize the strain effects of the (Δ_1^{lc}) conduction bands by introducing deformation potentials for the shifts and the splittings of the zone-center states Γ_{15}, $\Gamma_{2'}^{v}$, and $\Gamma_{2'}^{l}$ that constitute the Δ_1^{lc} states. We find that it is sufficient to describe a uniaxial and a hydrostatic deformation potential for the Γ_{15} triplet, to adequately describe the motion of the sixfold Δ_1^{lc} valleys with strain. Since we have transferred all strain effects into deformation potentials associated with threefold-degenerate zone-center states Γ_{15} (for the conduction band) and $\Gamma_{25'}$ (for the valence band), we are able to predict the variation of the $k_{\min}$ (minimum of the Δ_1^{lc} band) as a function of strain. Our calculations indicate that strain does not change $k_{\min}$ by more than 2–3 % of its unstrained value. However, the energies of the Δ_1^{lc} minima are affected substantially by [001] strain, which splits the original sixfold degeneracy into twofold longitudinal valleys and fourfold transverse valleys. Figure 1 shows the relative band alignments of a Si-$Si_{0.5}Ge_{0.5}$ superlattice grown on a Si-$Si_{0.75}Ge_{0.25}$ buffer layer. Most of our calculations of the band structure and optical properties are based on this superlattice.

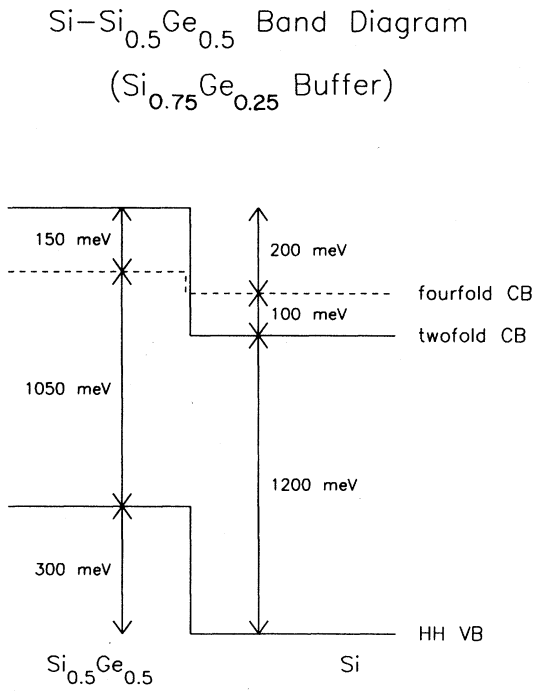

FIG. 1. Schematic diagram of a Si-$Si_{1-x}Ge_x$ superlattice band alignment indicating the relative positions of the twofold and fourfold conduction bands, and the heavy-hole valence bands. Strain distribution is calculated appropriate for pseudomorphic growth on a Si-$Si_{0.75}Ge_{0.25}$ buffer layer. These band alignments are based on the valence-band offset of Van de Walle. The conduction-band offset seen by the electrons belonging to the twofold valleys is 300 meV. The valence-band offset seen by the heavy holes is also 300 meV.

IV. BAND STRUCTURE

The superlattice band structure of the lowest conduction band of Si-$Si_{0.5}Ge_{0.5}$ was calculated using the four bulk states representing the $\pm k_{\min} \pm \Delta k$. The $k_{\min}$ is the position of the indirect minimum of the longitudinal conduction band. In our calculations of the superlattice conduction bands, we have neglected the two unphysical bands that are obtained from the diagonalization of the 6×6 companion matrix corresponding to the 3×3 Hamiltonian matrix given in Eq. (2). Similarly, only two bands have been retained for the calculation of the superlattice valence bands, since four of the six complex bands that are obtained from the 6×6 companion matrix related to the 3×3 Hamiltonian given in Eq. (3) correspond to unphysical solutions.

The most significant feature of the conduction band of indirect superlattices is that, due to the presence of the two longitudinal indirect valleys, the number of allowed solutions are doubled compared to the conduction band of a direct superlattice such as GaAs-$Al_xGa_{1-x}As$ ($x \leq 0.3$). Because of the interference between the electrons from the two longitudinal valleys, this additional degeneracy can be split and the lowest conduction band can then become a doublet that is slightly separated in energy. The actual splitting due to the interference effect is quite small (typically less than 10 meV). However, the magnitude of this splitting is a sensitive function of the layer thicknesses and the details of the matching conditions used; the envelope-function calculations give smaller interference effects than tight-binding calculations.[35] The interference effect in multivalley quantum-well structures has been studied by many investigators.[35–37] Our predictions on the interference effect in Si-$Si_{1-x}Ge_x$ are in qualitative agreement with the work of Chang and Ting.[35]

In Fig. 1 we have shown the band alignments of the Si-$Si_{0.5}Ge_{0.5}$ superlattice. The positions of the strain split lowest conduction-band edges are shown as the twofold and the fourfold conduction bands. The twofold bands are the longitudinal valleys with heavy effective masses along the growth direction with $k_{\parallel}=0$. The fourfold bands are the transverse ellipsoids in the x-y plane with $k_{\parallel}\neq0$. The well material for the conduction band of the superlattice is Si. In Si layers grown on buffer layers with a larger in-plane lattice constant, the twofold minima lie below the fourfold minima. In the barrier material $Si_{0.5}Ge_{0.5}$, this situation is reversed. For the rest of this paper we have assumed that the strain distribution of the superlattice is determined by setting the in-plane lattice

constant of each layer equal to that of the buffer layer. For superlattice layers that do not exceed the critical thickness,[38,39] this is a reasonable assumption.[40] However, since we have picked a buffer layer midway between Si and $Si_{0.5}Ge_{0.5}$, these results would also be applicable for free-standing superlattices with equal Si and $Si_{0.5}Ge_{0.5}$ layer thicknesses. By a free-standing superlattice we mean a configuration in which the in-plane lattice constant has been determined by minimizing the elastic free energy of the structure.[40]

We expect no coupling between the twofold and the fourfold valleys since $k_{\parallel}$ is conserved across the interface. Thus the barrier seen by the twofold states in going from Si to $Si_{1-x}Ge_x$ layers is ≈ 300 meV, although the lowest conduction state in the barrier is the fourfold minimum that is only 150 meV above the Si twofold states.[28] The heavy longitudinal masses of the twofold bands confines the superlattice states typically less than 100 meV from the bulk band edge. The fourfold states on the other hand have smaller effective masses, and the superlattice states lie above the fourfold band edge in strained Si. Thus, we can neglect the presence of the folded fourfold minima since they correspond to higher conduction states. Furthermore, one does not expect optical transitions from the fourfold minima since their $k_{\parallel}$ component does not get zone folded to Γ.

In a typical situation, the band structure of the Si-$Si_{0.5}Ge_{0.5}$ superlattice is expected to be indirect. For superlattices to be quasidirect, a special condition on the layer thicknesses has to be satisfied. To a crude approximation, we can derive the condition for such quasidirectness by considering that the conduction band of Si-$Si_{1-x}Ge_x$ superlattice to be composed of a slowly varying envelope function of the Kronig-Penney form, superimposed on top of a rapidly varying carrier wave that oscillates at $k_{\min}^{Si}$ or $k_{\min}^{Si_{1-x}Ge_x}$ in the appropriate layer. To achieve a quasidirect superlattice, the phase of the carrier wave should be roughly a multiple of 2π; more precisely, phase of the carrier wave should cancel with the phase of the envelope function at the end of a superlattice period. Thus we arrive at the approximate relation given in Eq. (1) for direct superlattices. This simple relation agrees remarkably well with the results of a more complicated analysis based on imposing the Bloch condition on the multicomponent envelope functions.

The character of the lowest conduction band in Si-$Si_{1-x}Ge_x$ superlattices can undergo significant changes for a layer thickness variation of 1–2 monolayers. To illustrate this, in Figs. 2(a), 2(b), and 2(c) we present how the superlattice band structure changes from a direct position in Fig. 2(a), to an indirect position where the lowest point of the conduction band is pinned at the Brillouin-zone edge in Fig. 2(c). The superlattices shown in Fig. 2 are assumed to be grown along the [001] direction. Our notation of an $n \times m$ superlattice defines a structure with n monolayers of Si, and m monolayers of $Si_{1-x}Ge_x$ within a single period. In Fig. 2(a) we have shown how a direct superlattice can be achieved with a 7.2 monolayer$\times$7.2 monolayer superlattice; since a 7$\times$7 superlattice is only approximately direct, we had to use fractional monolayers to achieve an illustrative direct superlattice.

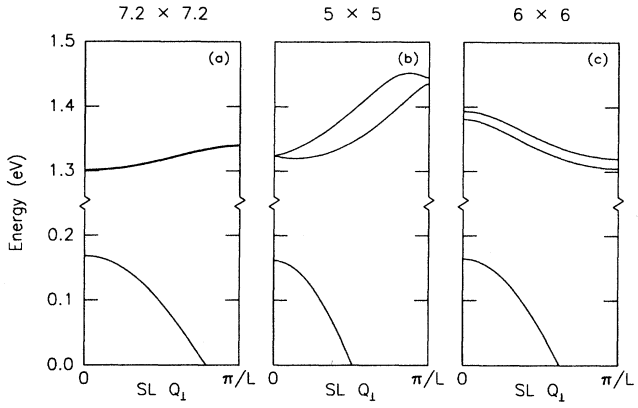

FIG. 2. Band structure of Si-$Si_{0.5}Ge_{0.5}$ superlattices for three illustrative layer thicknesses. The upper bands correspond to the longitudinal twofold conduction bands, and the lower bands correspond to the heavy-hole bands. Here, SL $Q_\perp$ denotes the superlattice wave vector and π/L denotes the edge of the reduced Brillouin zone. (a) shows a direct band structure corresponding to a 7.2$\times$7.2 monolayer superlattice. (b) shows the indirect band structure of a 5$\times$5 monolayer superlattice. (c) shows the indirect band structure of a 6$\times$6 superlattice where the minimum of the conduction band occurs at the edge of the reduced Brillouin zone.

In Si-$Si_{1-x}Ge_x$ superlattices when the layer thicknesses are approximately equal, and the band structure is almost quasidirect, the energy splitting of the lowest conduction-band doublet becomes very small (almost degenerate). However, if the barrier and the well have different thicknesses for a quasidirect superlattice, then the interference effect splits the almost-degenerate conduction band to a doublet slightly separated in energy [two direct bands analogous to Fig. 2(c)]. In Fig. 2(b) we show the band structure of a 5$\times$5 Si-$Se_{1-x}Ge_x$ superlattice. The splitting of the lowest conduction band into a doublet is clearly shown. For a direct material with the same effective mass, the corresponding superlattice band structure would be a single conduction band at the average position of the lowest two conduction bands shown. In this case, the minimum of the superlattice conduction band lies at an arbitrary point along the Δ axis. In Fig. 2(c) we show a 6$\times$6 superlattice which has the conduction-band minimum at the reduced zone boundary. Again, the conduction band appears as a doublet due to the interference effect. In Fig. 2 we have also shown the band structure of the corresponding heavy-hole state. The dispersion is less for the conduction bands (≈ 100 meV) because of their higher effective masses. However, it should be noted that even when varying the layer thicknesses by a small amount as from 5 to 7 monolayers, the band structure of the superlattice conduction band changes quite significantly, in contrast to the valence band that stays almost the same. This has the implication that, to achieve a given band structure, it is important to control the layer thicknesses to roughly within a monolayer.

The optical band gap of Si-$Si_{1-x}Ge_x$ superlattices de-

pends on the positions of the heavy-hole state and the lowest conduction states. In Fig. 3 we present the heavy-hole valence-band position as a function of the Si and $Si_{0.5}Ge_{0.5}$ layer thicknesses. We have assumed that the in-plane lattice constant is set by the $Si_{0.75}Ge_{0.25}$ buffer layers. The valence-band offset for Fig. 3 is $E_V^{Si_{0.5}Ge_{0.5}} - E_V^{Si} = 300$ meV. Since the Si layers act as the barrier material for the heavy-hole band, the effect that the Si layer thickness has on the position of the heavy-hole band is quite small. Thus the motion of the valence-band edge position is mainly due to the variation of the layer thicknesses of the $Si_{0.5}Ge_{0.5}$ layers. The zero of energy for the contour lines of Fig. 3 is the position of the heavy-hole band of the Si layer. On the other hand, Fig. 4 shows the energy of the lowest superlattice conduction-band state as a function of the layer thicknesses. The conduction-band offset for Fig. 4 is $E_C^{Si_{0.5}Ge_{0.5}} - E_C^{Si} = 300$ meV. This corresponds to the band offset between the twofold minima. The zero of energy for the contours of Fig. 4 is still the position of the heavy-hole band of the Si layers. The bottom of the well (conduction band of Si) lies at 1.2 eV and the top of the barrier (conduction band of $Si_{0.5}Ge_{0.5}$) lies at 1.5 eV. Since $Si_{0.5}Ge_{0.5}$ layers act as the barrier material for the conduction band, the effect its layer thickness has on the position of the conduction band is quite small. Thus the motion of the conduction-band edge position is predominantly due to the layer-thickness variations of the Si layer. However, notice that the variation in energy for the conduction-band states is considerably less than in the case of the valence-band states of Fig. 3. This is because

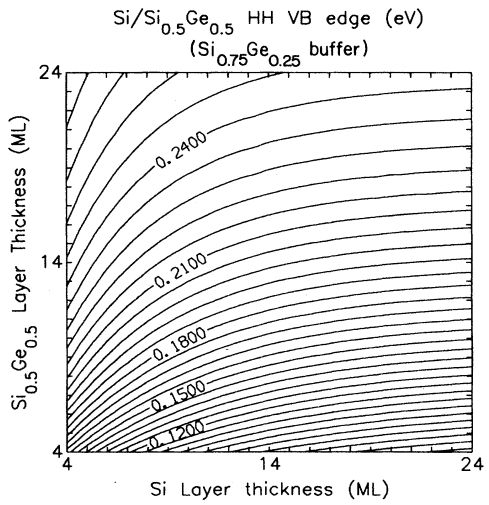

FIG. 3. Contour plot of the Si-$Si_{0.5}Ge_{0.5}$ superlattice valence-band edge (heavy hole) position as a function of the layer thicknesses of Si and $Si_{0.5}Ge_{0.5}$ within a single superlattice period. The valence-band offset seen by the heavy holes is assumed to be 300 meV. The strain distribution corresponds to a Si-$Si_{0.5}Ge_{0.5}$ superlattice grown pseudomorphically on a S-$Si_{0.75}Ge_{0.25}$ buffer layer. The zero of energy corresponds to the unstrained position of the heavy-hole band edge of pure Si (see Fig. 1) (ML=monolayer).

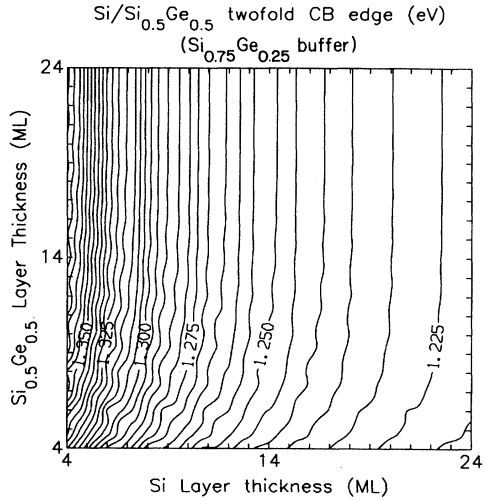

FIG. 4. Contour plot of the Si-$Si_{0.5}Ge_{0.5}$ superlattice conduction-band (twofold) edge as a function of the layer thicknesses of Si and $Si_{0.5}Ge_{0.5}$ within a single superlattice period. The valence-band offset seen by the twofold states is assumed to be 300 meV. The strain distribution corresponds to a Si-$Si_{0.5}Ge_{0.5}$ superlattice grown pseudomorphically on a Si-$Si_{0.75}Ge_{0.25}$ buffer layer. The zero of energy corresponds to the unstrained position of the heavy-hole band edge of pure Si (see Fig. 1).

of the large effective mass associated with the conduction band.

Due to the interference effect, the actual minimum of the lowest conduction band gets shifted up or down depending on the layer thicknesses. This can be seen from Fig. 4 as the small oscillations in the contour curves roughly parallel to the lines of constant $k_{\min}^{Si} d^{Si} + k_{\min}^{Si_{1-x}Ge_x} d^{Si_{1-x}Ge_x}$. It should be noted that as the well (Si layer) width increases, the effects due to the interference effect also get reduced. The actual shift in energy due to the interference effect typically does not exceed 10 meV, and decreases with the increase of the well widths as $1/L_W^3$.[16] Here, L_W is the well width within a single repeat of the superlattice.

Although the interference effect leads to small shifts in energy, it dominates the determination of the position in Q where the minimum of the folded conduction band occurs. On a contour plot of d^{Si} and $d^{Si_{0.5}Ge_{0.5}}$, the domain for obtaining quasidirect superlattices can be expected to be a family of lines such as in Eq. (1). However, in our model the interference effect gives rise to a width for these lines, thus enhancing the domain for obtaining quasidirect superlattices to a two-dimensional subspace. Theoretically it is now possible to achieve an exactly direct superlattice by tailoring the layer thicknesses to lie within one of these two-dimensional domains. The details of the width of the strips that give rise to direct band structure on a contour plot of and d^{Si} and $d^{Si_{1-x}Ge_x}$ is a sensitive function of the matching condition. The problem of achieving exactly direct band structure is only of academic interest. In reality, it is adequate to achieve ap-

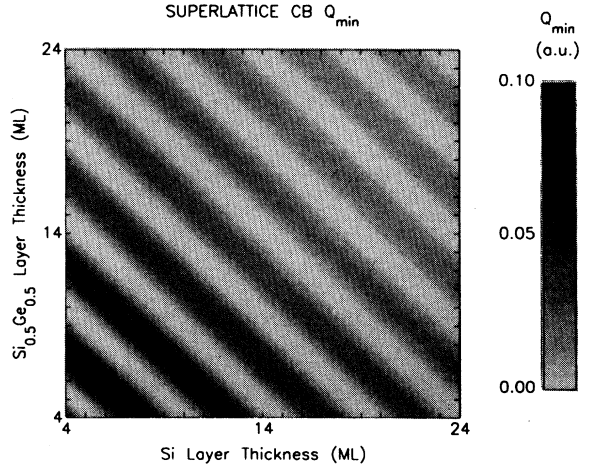

FIG. 5. Gray scale plot of $Q_{\min}$ (wave vector of the lowest conduction state) as a function of the layer thicknesses of Si and $Si_{0.25}Ge_{0.25}$ within a single period of the superlattice. Here, $Q_{\min}$ is in atomic units. For comparison the Brillouin zone edges of Si and $Si_{0.5}Ge_{0.5}$ in the [001] direction have wave vectors 0.612 and 0.587 in atomic units (1/bohr). The series of light strips corresponds to roughly direct band structure while the darker regions correspond to indirect band structure. This figure shows excellent agreement with the qualitative prediction of Eq. (1).

proximately direct superlattices, since transitions are allowed from each point along the folded valence band to the corresponding point in the conduction band. The contour plot of Fig. 5 shows the wave vector for the minimum position of the conduction band based on the matching of the zone-center components across the interface. The lighter regions correspond to approximately direct superlattices. The darker regions correspond to situations when the minimum of the conduction band occurs closer to the reduced zone edge. The results of Fig. 5 clearly indicate that one obtains quasidirect and/or indirect superlattices in strips of the layer-thickness space. This verifies our prescription for quasidirect superlattices based on Eq. (3). It should also be noted that the wave vector shown in Fig. 5 is in atomic units (1/bohr). The wave vectors get smaller as the layer thicknesses are increased since the size of the Brillouin zone is proportional to $\pi/(d^{\mathrm{Si}}+d^{\mathrm{Si_{0.5}Ge_{0.5}}})$.

V. OPTICAL PROPERTIES

While a direct band gap is necessary for good optical absorption, it is not sufficient. We also need a finite value of the optical matrix element. In this section we present the theory for the calculation of the optical properties. The optical absorption is proportional to the square of the momentum matrix element between the conduction and the valence bands. The optical matrix element M_{op} between a valence state of k_v and a conduction state of k_c can be written as

$$M_{\mathrm{op}}=\int_L \langle u_c|\mathbf{p}|u_v\rangle e^{i(k_v-k_c)z}dz \ . \tag{4}$$

The optical matrix element is related to the imaginary part of the dielectric function $\epsilon_2(\omega)$ by

$$\epsilon_2(\omega)=\sum \mathcal{A}\,|M_{\mathrm{op}}|^2\frac{1}{\omega^2}(\omega-\omega_0)^{1/2} \ , \tag{5}$$

if a parabolic density of states is assumed. The constant $\mathcal{A}$ is given by

$$\mathcal{A}=2e^2\hbar^{1/2}/m^2(2m^*/\hbar^2)^{3/2} \ . \tag{6}$$

The integration domain of (4) is over the whole length of the crystal. In Eq. (5) the sum is over all the bands that contribute to optical transitions at the appropriate energy. The quantities ω and ω_0 are the energies of the incident radiation and the band gap. In Eq. (6) m^* is the combined density of states mass.[41] In the case of an indirect transition, Eq. (5) has to be modified since the combined density of states is no longer parabolic.

In Eq. (4) u_c and u_v are the periodic parts of the Bloch functions corresponding to the conduction and valence states. They are rapidly varying functions on a scale smaller than a monolayer, and can be expanded in terms of the zone-center $\mathbf{k}\cdot\mathbf{p}$ basis set. Since the representation for the momentum operator in the zone-center basis set is known, the matrix element $\langle u_c|\mathbf{p}|u_v\rangle$ over a unit cell can be evaluated easily. Here u_v and u_c are wave functions normalized over a unit cell of the bulk. The resulting expression can then be written as

$$M_{\mathrm{op}}=M'_{\mathrm{op}}\int e^{i(k_v-k_c)z}dz \ , \tag{7}$$

where we have taken the rapidly varying $\langle u_c|\mathbf{p}|u_v\rangle$ part of the integrand outside the integral, and replaced it with its average over a unit cell

$$M'_{\mathrm{op}}=\langle u_c|\mathbf{p}|u_v\rangle \ . \tag{8}$$

$|M'_{\mathrm{op}}|^2$ is related to the optical absorption strengths of the bulk materials. The integral in Eq. (7) becomes a δ function of (k_v-k_c) when integrated over the length of the crystal. This is the familiar k conservation condition for optical transitions between different bands (assuming that photons have negligible k). In bulk Si and Ge, the matrix element between the periodic part of the Bloch function $\langle u_c|\mathbf{p}|u_v\rangle$ is nonzero for x and y polarizations for transitions from the [001] valleys to the top of the valence bands although the k conservation condition is not satisfied. Thus, it would be possible to observe these transitions in a direct $Si\text{-}Si_{1-x}Ge_x$ superlattice where the k conservation condition is satisfied.

In a superlattice, the corresponding change to (7) and (8) are

$$M^{\mathrm{SL}}_{\mathrm{op}}=\int_L \langle U_c(z)|\mathbf{p}(z)|U_v(z)\rangle e^{i(k_v^{\mathrm{SL}}-k_c^{\mathrm{SL}})z}dz \ . \tag{9}$$

Here, $U_c(z)$ and $U_v(z)$ are the envelope functions that are periodic on the scale of a superlattice unit cell. We can first perform the integrations over a unit cell of the superlattice to obtain

$$M^{\mathrm{SL}}_{\mathrm{op}}=M'^{\mathrm{SL}}_{\mathrm{op}}\int_L e^{i(k_v^{\mathrm{SL}}-k_c^{\mathrm{SL}})z}dz \ , \tag{10}$$

where

$$M_{\rm op}'^{\rm SL} = \langle U_c(z)|\mathbf{p}(z)|U_v(z)\rangle \ . \tag{11}$$

The strength of the optical transitions is then related to $|M_{\rm op}'^{\rm SL}|^2$. These envelope functions are normalized to a single unit cell of the superlattice. It is possible to achieve $K_v^{\rm SL}=k_c^{\rm SL}$ condition at energies fairly close to the band edges, in superlattices approximately satisfying the quasidirect conduction given in Eq. (1).

In Fig. 6(a) we have shown the typical charge density of the wave function at the conduction-band edge (from the indirect band edge of a 5×5 superlattice). This wave function is composed of a rapidly varying carrier wave that is superimposed on top of a slowly varying envelope function that mimics a conventional Kronig-Penny solution. However, only the valence-band wave function has a slowly varying envelope function as shown in Fig. 6(b). Thus, the coupling between these states through the momentum matrix element is quite small. These wave functions essentially have different Fourier components and are still almost orthogonal in spite of the band folding. Thus, in a typical situation, $M_{\rm op}'^{\rm SL}$ evaluates to a small number less than 10^{-2} (atomic units). Thus in comparison to the square of the optical matrix element of bulk GaAs $|M_{\rm op}|^2 \approx 1.8$ a.u.,[42] the direct absorption strengths of Si-$Si_{1-x}Ge_x$ superlattices are 3–4 orders of magnitude smaller.

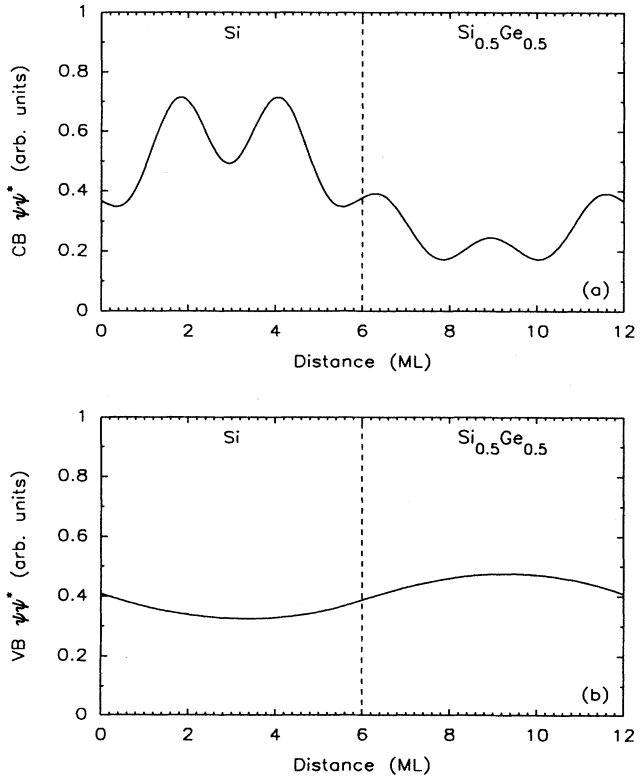

FIG. 6. The charge density of the superlattice envelope functions corresponding to a 6×6 Si-$Si_{0.5}Ge_{0.5}$ structure. The conduction band $\psi\psi^*$ can have rapid oscillations compared to the valence band. The $\psi\psi^*$ of these wave functions were normalized to a superlattice unit cell. The **p** matrix elements between the conduction- and valence-band wave functions can be expected to be quite small since they have different Fourier components.

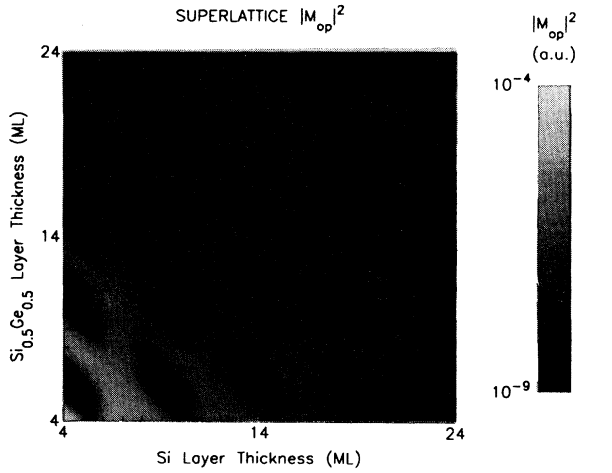

FIG. 7. Gray-scale plot of the $|M_{\rm op}|^2$ (square of the optical matrix element) as a function of the layer thicknesses of Si and $Si_{0.5}Ge_{0.5}$ within a single period of the superlattice. Here, $|M_{\rm op}|^2$ is in atomic units. For comparison bulk GaAs has a $|M_{\rm op}|^2$ of 1.86. The darker regions have the enhanced optical matrix elements. In this figure it is clearly seen that layer-thickness variations of 1–2 monolayers can change the optical matrix elements by 3–4 orders of magnitude.

In Fig. 7 we have shown the square of the optical matrix element versus the layer thicknesses for the transition from the lowest conduction-band state to the corresponding valence-band state. The expected matrix elements are quite small as explained in the previous section. However, the major contribution to the optical matrix element integral comes from the interfaces. Thus, the phase of the conduction-band wave function at each interface plays an important role in determining this quantity. As seen in Fig. 7 we see that changing the layer thicknesses of either layer by approximately 2–3 monolayers (phase change of π) changes the absorption strength from darker regions to lighter regions and vice versa. Thus, the optical absorption strength of Si-$Si_{1-x}Ge_x$ superlattices is a very sensitive function of the layer thickness. The maximum optical matrix elements occurs at small layer thicknesses where a large interface to volume ratio exists. As the layer thicknesses are increased, the optical matrix elements decrease because the interface to volume ratio in the superlattice decreases. In the parameter space of 4–24 monolayers, the maximum optical absorption strengths seem to occur at near 7×7 Si-$Si_{1-x}Ge_x$ superlattice.

VI. CONCLUSION

We have presented a theory for the calculation of the band structure and the optical properties of the Si-$Si_{1-x}Ge_x$ superlattices based on the envelope-function approximation. We have shown how the band structure

of indirect superlattices such as Si-$Si_{1-x}Ge_x$ can be tailored to obtain roughly direct band gaps by following a simple prescription such as Eq. (1). We have also shown that only the p_x and p_y polarizations are allowed for optical transitions between the conduction and valence bands of such direct superlattices grown along the [001] direction. The optical absorption strengths associated with these new quasidirect transitions can be 3–4 orders of magnitude larger than the phonon-assisted absorption strengths of pure Si or Ge. However, the band folded states have much weaker optical absorption properties compared to the absorption from direct materials ($\approx$3 orders of magnitude lower). It is important to control the layer thicknesses fairly accurately (up to a single monolayer accuracy) to achieve the enhanced optical absorption.

ACKNOWLEDGMENTS

This work was supported by the Defense Advanced Projects Agency, U.S. Department of Defense, under Contract No. N00014-86-K-0841. We would also like to acknowledge useful discussions with R. H. Miles, R. J. Hauensetin, D. Z. Ting, and O. J. Marsh.

[1]K. E. Peterson, Proc. IEEE **70**, 420 (1982).
[2]S. M. Sze, *Physics of Semiconductor Devices* (Wiley, New York, 1981).
[3]L. Esaki and R. Tsu, IBM J. Res. Dev. **40**, 61 (1970).
[4]R. Hull, J. M. Gibson, and J. C. Bean, Appl. Phys. Lett. **46**, 179 (1985).
[5]R. People, J. C. Bean, D. V. Lang, A. M. Sergent, H. L. Stormer, K. W. Wecht, R. T. Lynch, and K. Baldwin, Appl. Phys. Lett. **45**, 1231 (1984).
[6]J. C. Bean, L. C. Feldman, A. T. Fiory, S. Nakahara, and I. K. Robinson, J. Vac. Sci. Technol. A **2**, 434 (1984).
[7]H. M. Manasevit, I. S. Gergis, and A. B. Jones, Appl. Phys. Lett. **41**, 464 (1982).
[8]E. Kasper and J. C. Bean, *Silicon Molecular Beam Epitaxy* (Chemical Rubber, Boca Raton, FL, 1987).
[9]S. A. Jackson and R. People, in *Materials Research Society Symposium Proceedings* (MRS, Pittsburgh, 1986), Vol. 56, p. 365.
[10]J. C. Bean, *Materials Research Society Symposium Proceedings* (MRS, Pittsburgh, 1985), Vol. 37, p. 245.
[11]M. S. Hybertsen and M. Schluter, Phys. Rev. B **36**, 9683 (1987).
[12]S. Satpathy, R. M. Martin, and C. G. Van de Walle, Phys. Rev. B **38**, 13 237 (1988).
[13]S. Ciraci and T. P. Batra, Phys. Rev. B **38**, 1835 (1988).
[14]S. Froyen, D. M. Wood, and A. Zunger, Phys. Rev. B **37**, 6893 (1988).
[15]M. Cardona and F. H. Pollack, Phys. Rev. **142**, 530 (1966).
[16]C. M. Sterke and D. G. Hall, Phys. Rev. B **35**, 1380 (1987).
[17]D. L. Smith and C. Mailhiot, Phys. Rev. B **33**, 8345 (1986).
[18]Y. C. Chang and J. N. Schulman, Phys. Rev. B **25**, 3975 (1982).
[19]M. F. H. Schuuraman and G. W. 't Hooft, Phys. Rev. B **31**, 8041 (1985).
[20]J. N. Schulman and Y. C. Chang, Phys. Rev. B **24**, 4445 (1981).
[21]T. F. Keuch, M. Mäenpää, and S. S. Lau, Appl. Phys. Lett. **39**, 245 (1981).
[22]G. Margaritondo, A. D. Katnani, N. G. Stoffel, R. R. Daniels, and Te-Xiu Zhao, Solid State Commun. **43**, 163 (1982).
[23]P. H. Mahowald, R. S. List, W. E. Spicer, and P. Pianetta, J. Vac. Sci. Technol. B **3**, 1252 (1985).
[24]W. A. Harrison, *Electronic Structure and Properties of Solids* (Freeman, San Francisco, 1980).
[25]J. Tersoff, Phys. Rev. B **30**, 4874 (1984).
[26]W. A. Harrison and J. Tersoff, J. Vac. Sci. Technol. **4**, 1068 (1986).
[27]C. G. Van de Walle and R. M. Martin, J. Vac. Sci. Technol. B **3**, 1256 (1985).
[28]C. G. Van de Walle and R. M. Martin, Phys. Rev. B **34**, 5621 (1986).
[29]R. People, Phys. Rev. B **32**, 1405 (1985).
[30]R. People and J. C. Bean, Appl. Phys. Lett. **48**, 538 (1986).
[31]G. L. Bir and G. E. Pikus, *Symmetry and Strain Induced Effects in Semiconductors* (Keter, Jerusalem, 1974).
[32]H. Hesagawa, Phys. Rev. **129**, 1029 (1962).
[33]J. C. Hensel and G. Feher, Phys. Rev. **129**, 1041 (1963).
[34]I. Balslev, Phys. Rev. **143**, 636 (1966).
[35]Y. C. Chang and D. Z. Ting, J. Vac. Sci. Technol. B **1**, 435 (1983).
[36]M. Nakayama and L. J. Sham, Solid State Commun. **26**, 6 (1978).
[37]L. J. Sham and M. Nakayama, Surf. Sci. **73**, 272 (1978); Phys. Rev. B **20**, 734 (1979).
[38]J. W. Matthews and A. E. Blakeslee, J. Cryst. Growth **27**, 118 (1974).
[39]R. People and J. C. Bean, Appl. Phys. Lett. **47**, 322 (1985).
[40]R. H. Miles, T. C. McGill, S. Sivananthan, X. Chu, and J. P. Faurie, J. Vac. Sci. Technol. B **5**, 1263 (1987).
[41]C. W. Higginbotham, M. Cardona, and F. H. Pollack, Phys. Rev. **184**, 821 (1969).
[42]C. W. Higginbotham, Ph.D. thesis, Brown University, Providence, RI, 1970.

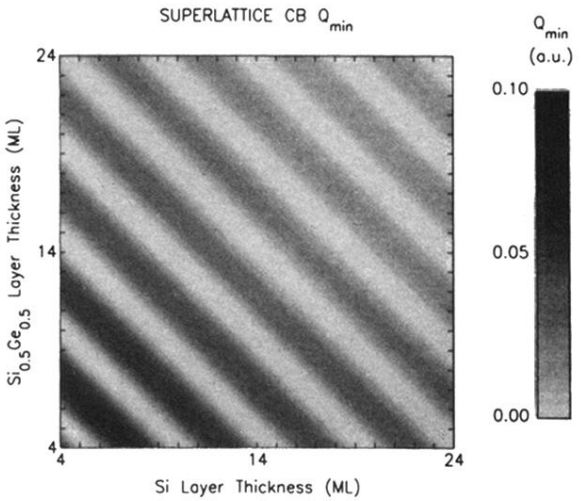

FIG. 5. Gray scale plot of Q_{min} (wave vector of the lowest conduction state) as a function of the layer thicknesses of Si and $Si_{0.25}Ge_{0.25}$ within a single period of the superlattice. Here, Q_{min} is in atomic units. For comparison the Brillouin zone edges of Si and $Si_{0.5}Ge_{0.5}$ in the [001] direction have wave vectors 0.612 and 0.587 in atomic units (1/bohr). The series of light strips corresponds to roughly direct band structure while the darker regions correspond to indirect band structure. This figure shows excellent agreement with the qualitative prediction of Eq. (1).

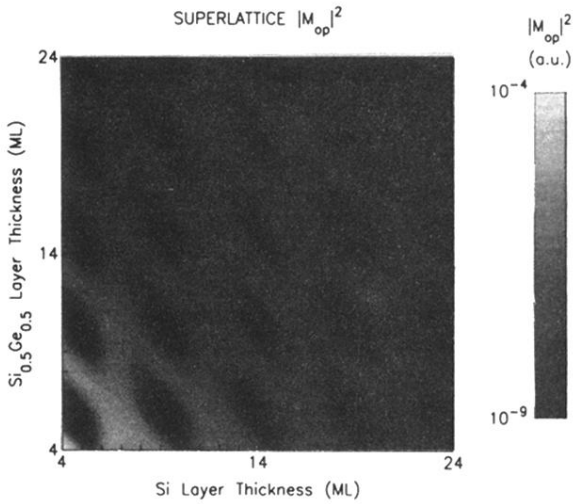

FIG. 7. Gray-scale plot of the $|M_{op}|^2$ (square of the optical matrix element) as a function of the layer thicknesses of Si and $Si_{0.5}Ge_{0.5}$ within a single period of the superlattice. Here, $|M_{op}|^2$ is in atomic units. For comparison bulk GaAs has a $|M_{op}|^2$ of 1.86. The darker regions have the enhanced optical matrix elements. In this figure it is clearly seen that layer-thickness variations of 1–2 monolayers can change the optical matrix elements by 3–4 orders of magnitude.